Peer-reviewed version available at *Minerals* **2020**, *10*, 708; doi:10.3390/min10080708

Article

Genesis of Two Types of Carbonaceous Material and Associated with Gold Mineralization in the Bumo Deposit, Hainan Province, South China

Zhengpeng Ding[1, 2], Teng Deng[1, 2, *], Deru Xu[1, 2], Zenghua Li[1, 2], Shaohao Zou[1, 2], Lirong Li[1, 2], Ke Xu[1, 2], Yan Hai[1] and [2]

[1] State Key Laboratory of Nuclear Resources and Environment, East China University of Technology, Nanchang 330013, China
[2] School of Earth Sciences, East China University of Technology, Nanchang 330013, China
* Correspondence: dengteng2015@ecut.edu.cn (T.D.); Tel.: +86-13533681792

Abstract: Carbonaceous material (CM) is common in meta-sediments and is generally interpreted to be intimately associated with gold mineralization. For the Bumo deposit in Hainan Province, South China, CM is mainly hosted by greenschist facies- to amphibolite-facies metamophic rocks of the Paleo- to Mesoproterozoic Baoban Group and by auriferous veins and is used as an important gold prospecting indicator. However, the genesis of CM and the relationship with gold mineralization are still not clear. Field work and thin section observation indicates that two types of CM occur, i.e., layered and veinlet. Layered CM, up to meters thick, prevails in the deposit. More importantly, Au-bearing sulfides are commonly distributed along the boundary between the quartz veins and layered CM. In contrast, veinlet CM, co-precipitated with gold and sulfides, has the thickness of micro- to centi- meters, and these thin veins occur in quartz veins and hydrothermally altered rocks. Scanning Electron Microscope (SEM) analysis indicates that layered CM has a stringy shape and laminate structure, while veinlet CM occurs as isometric particles. Raman carbonaceous material geothermometer indicates that layered CM with high maturity is formed at elevated temperatures of 400 – 550°C, consistent with X-ray diffraction (XRD) analysis. In contrast, veinlet CM with low maturity is formed at 200 – 350°C, generally consistent with gold mineralization. In addition, layered CM has $\delta^{13}C$ values ranging from -30 to -20%, demonstrating a biogenic origin. Consequently, it is interpreted that layered CM is formed by a pre-ore metamorphic event during Caledonian, and its reducing nature promotes gold precipitation via destabilization of aqueous Au bisulfide complexes or facilitating sulfidation. Veinlet CM is hydrothermal origin, and its precipitation modified the chemical conditions of ore fluids, leading to the destabilization of Au complexes and thus favorable for mineralization.

Keywords: Carbonaceous material; Raman Geothermometer; Au; gold deposit; Hainan

1. Introduction

Carbonaceous material (CM) was reported to be found in many metasediment-hosted orogenic gold deposits, such as the Macraes deposit in New Zealand [1], Cosmo Howley in Australia [2], and Syama, Obuashi and Inata deposits in west Africa [3]. Previous studies proposed that CM can be generated by metamorphic and hydrothermal activities [4]. The relationships between CM and gold mineralization have been proposed to be: 1) pre-mineralization CM as reducing agent to cause the precipitation of Au and sulfides [5], 2) pre-mineralization CM absorbing Au and leached by syn-ore fluids[6], 3) pre-mineralization CM as physically weak part to facilitate shear zones that localize ore veins [7] and 4) syn-mineralization CM co-precipitated with gold and sulfides due to hydrothermal activities [8].

Peer-reviewed version available at Minerals 2020, 10, 708; doi:10.3390/min10080708

CM is widely distributed in the NE-trending Gezheng shear zone, the most important gold mineralization area in Hainan Province, South China [9]. CM-bearing rocks mainly include mylonite, compound gneiss and schists in Precambrian metasediments, and they are especially common in many gold deposits, such as the Bumo, Beiniu, Baoban, Fengshuishan and Baolun deposits [10]. Previous research suggests that CM in the Baoban Group is produced by regional metamorphism [9], and some of them are used for gold prospecting indicators. However, no studies have been conducted on the geological and geochemical characteristics of CM, so the genesis and association with gold mineralization are still not clear.

The Bumo deposit, with the Au reserve of about 13t and an average grade of 9.97 g/t, is hosted by metasediments in the Paleo- to Mesoproterozoic Baoban Group. Among all the gold deposits along the Gezhen shear zone, the Bumo deposit is the one closest correlated with CM-bearing rocks. Major ore veins are located near CM, and the gold grade in individual veins is strongly affected by amount of CM [11,12]. However, the CM in the Bumo deposit has never been studied previously. CM characteristics in terms of structure, maturity, temperature and isotopic composition are still not clear. Therefore, its contributions to auriferous veining are still not well understood. This paper uses an integrated analytical approach, combined field and petrographic work, SEM, Laser Raman, XRD and carbon isotope, to identify the two types of CM and their genesis and relationships with the gold mineralization in the Bumo deposit.

2. Regional Geology

The Hainan Province (Hainan Island), an epicontinent-type island in the north of the South China Sea, is situated at the conjunction part among the Pacific, Eurasian, and Indo-Australia plates (Figure 1A) [13,14]. The tectonic movements are divided into six stages with ages of Jinningian, Caledonian, Hercynian, Indosinian, Yanshanian, and Himalayan time [15,16]. The tectonic events produced two major sets of structures, i.e., EW- and NE-trending faults. Among them, the EW-trending structures mainly include the Wangwu-Wenjiao, Changjiang-Qionghai, Jianfeng-Diaoluo, and Jiusuo-Lingshui faults, while the NE-trending structures, represented by the Gezhen and Baisha shear zones (Figure 1B) [17,18].

The Proterozoic strata in Hainan Province are well-developed (Figure 1B), including Mesoproterozoic Baoban Group (ca. 1.8 – 1.45 Ga); [16], Meso-Neoproterozoic Shilu Group (ca. 1075 – 880 Ma); [19] and Neoproterozoic-Sinian Shihuiding Formation [12]. The Baoban Group predominantly distributed in the central Hainan Province, is composed of migmatitic gneisses, black shales, plagioclase-amphibole gneisses, and quartz-muscovite schists with amphibolite to granulite facies metamorphism [9,20]. The Shilu Group, distributed located in the west Hainan, consists of a set of shallow sea-lagoon facies (iron-bearing) volcanic-clastic rocks, carbonaceous shales and black shales. The contact between the Baoban Group and the overlying Shilu Group is hard to observed due to the cover of the Quaternary sediments [16,17]. The Shihuiding Formation consists of black slates, quartz sandstones and quartzites intercalated with siltstones [14]. There is an unconformable contact between the Shilu Group and Shihuiding Formation [16,21]. The Precambrian rocks in Hainan likely went through an extensive regional metamorphism during Caledonian [22].

It is noteworthy to mention that all the Precambrian metasediments are characterized with high contents of CM, up to volumetrically >10%, and it is hosted in the black shales, slates and carbonaceous shales, carbonaceous phyllites and carbonaceous mudstones [12,16,17]. These carbonaceous rocks commonly occur over many tens of kilometers rock band in the central Hainan Province [23].Previous research indicates that CM is likely to be generated by metamorphism during Caledonian period, and soured from Precambrian [24].

The exposed intrusive rocks account for about 40% of the land area, mostly located in western-central Hainan Province. Most of those intrusions were produced at Yanshanian (175 – 65 Ma) and Hercynian-Indosinian (ca. 300 – 200 Ma) time [25], and the corresponding rocks are monzogranites-granodiorites and alkaline granites, respectively (Figure 1B). Late Paleozoic to early Mesozoic I-type granites are the most common and marked the beginning of the South China Indosinian Orogeny whereas the late Mesozoic calc-alkaline granites are considered as a response to the subduction of the

Paleo-Pacific plate [26]. A few Mesozoic and Cenozoic basalts outcropped in several rift basins in northern Hainan Province [27].

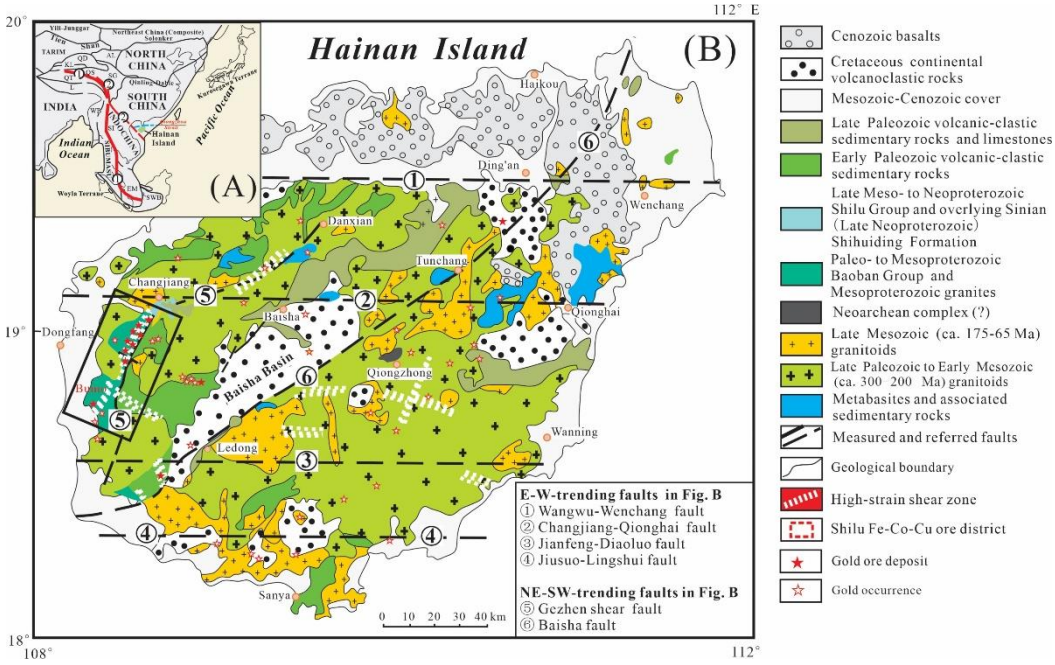

Figure 1. (A) Location map of Hainan Island (modified after Xu et al. 2017[12]); (B) Schematic diagram showing the main strata and magma units, gold deposits and occurrences in the Hainan Island, South China (modified after Xu et al. 2017[12]).

More than 50 gold deposits and occurrences with a gold reserve of over 143 t have been discovered in Hainan Province, and most of them are located along the Gezhen ductile shear zone. The Gezhen ductile shear zone predominantly occurred as a narrow and long area, extending more than 150 kilometers in central western Hainan Province [25]. The shear zone is characterized by multi-episodic tectonism, including earlier brittle-ductile and later ductile-brittle shearing deformation [19]. The major gold deposits in the Gezhen ductile shear zone are represented by the Bumo, Beiniu, Tuwaishan, Baoban, Niuling and Erjia deposits [25]. CM-bearing rocks are important host rocks for Au in Gezhen gold deposits, and the rocks mainly include carbonic phyllites, black shales, and carbonaceous slates [11].

3. Ore Deposit Geology

The Bumo gold deposit is situated in the southwestern part of the DongFang city, Hainan Province, and has an area of 56 km^2 [28]. The rocks in the Bumo deposit include the Baoban, Shilu groups and Quaternary sediments (Figure 2A). The Baoban Group is mainly composed of the quartz sericite schists, carbonaceous shales (CM-bearing rock), metamorphosed quartzose sandstones, phyllites, migmatization schists. The Shilu Group consists mainly of the metamorphosed quartzose sandstones, biotite adamellites, carbon slates (CM-bearing rock) and mylonite schists. The Quaternary loose sediments are mainly composed of unconsolidated sediments of sand [25]. CM -bearing rocks are quite common within the Baoban and Shilu groups in the Bumo deposit, such as carbonaceous phyllites, carbonaceous mudstones and shales [12]. Locally, CM was aggregated along faults to form CM layer with the thickness up to one meter, and they are commonly associated with gold-quartz veins [12,19].

Magmatic rocks are not common in the mining area, only have a few Hercynian and Indosinian period monzogranites exposure to the southern side of the deposit [25]. Even though the possible existence of concealed intrusions is suggested by Controlled Source Audio-Frequency Magotelurics (CSAMT), and Audio-Frequency Magotelurics (AMT). There are some Yanshanian pegmatite, diorite porphyry, and diorite outcrop outside in the north of the deposit area [4]. There are three sets of faults

in the deposits i.e., the NE-, NW- and EW-trending faults, which host gold-bearing quartz veins, and parallel to the host rock of the Baoban Group [29,30]. The NW- and EW-trending faults cut through the NE-trending faults, suggesting that the NW- and EW-trending faults formed after the NE-trending faults [20].

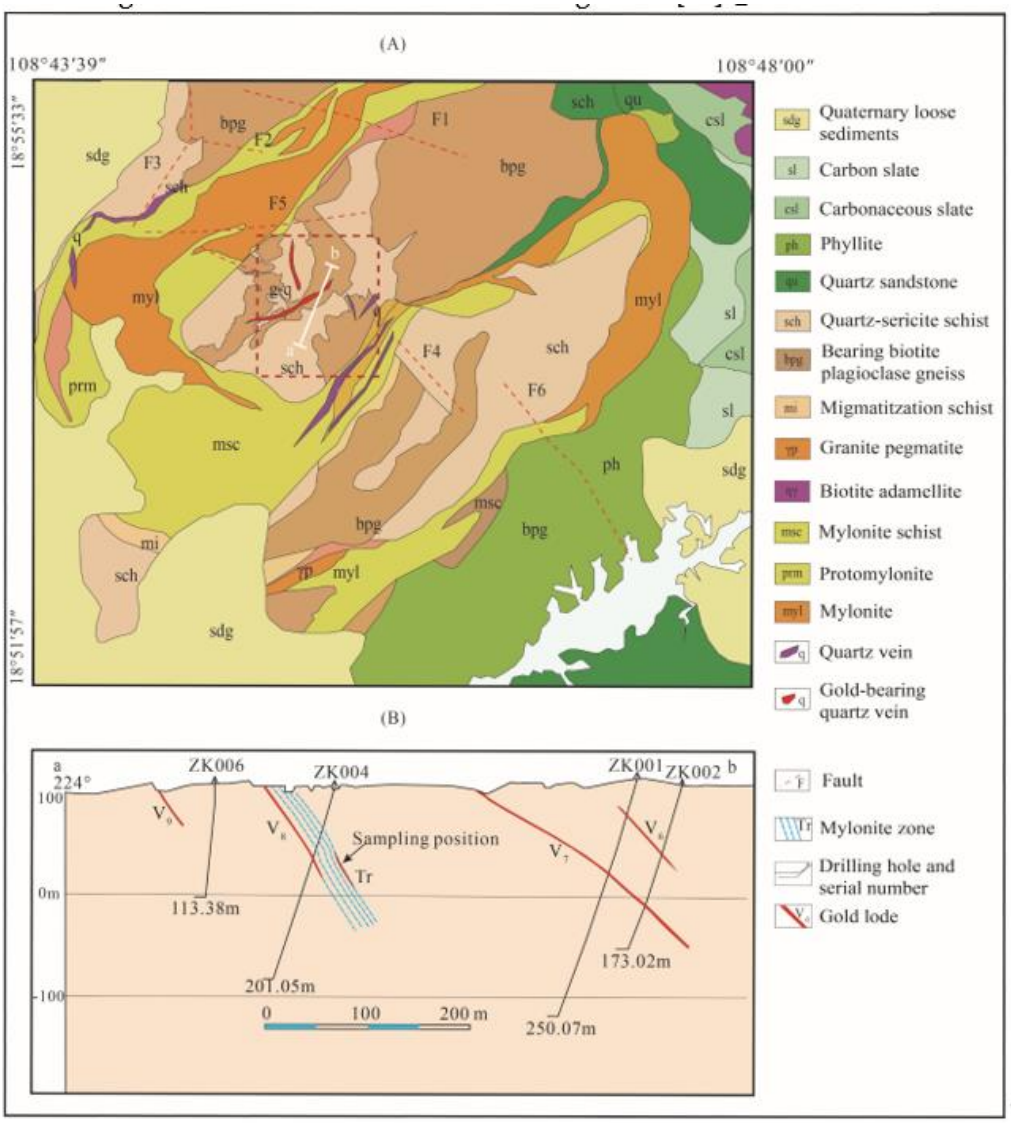

Figure 2. Simplified geological map showing the location of the gold deposits in the Gezhen brittle-ductile shear zone, western Hainan (modified after Xu et al. 2017[12]) .

More than 20 orebodies have been discovered in the Bumo deposit. Most orebodies are irregular lodes controlled by the fault, which generally occurring SW–trending fault and parallel to each other (Figure 2A). The No. 2 orebody, consisting of V6-V9 lodes in the center of the Bumo deposit, is the ore vein with the largest tonnage (Figure 2B). This orebody dips at 90°–97°to the SW and has an average ore grade of 5 g/t Au. Two mineralization styles are recognized, i.e., disseminated and vein type ores [11]. Wall rock alteration mainly includes pyritization, silicification and sericitization [10]. Pyrite and arsenopyrite are the two principal ore minerals (Figure 3A), and there are also some sphalerite, chalcopyrite and galena (Figure 3B). The gangue minerals mainly include quartz, CM, calcite and sericite (Figures 3C-D). Previous research indicates that the hydrothermal event can be divided into three stages [4], i.e., quartz (Q1)-pyrite, quartz (Q2)-sulfides and quartz (Q3)-calcite stages, with the second stage as the main mineralization stage. Different from the white quartz (Q1) with euhedral structures (Figure 3E), Q2 grains are generally anhedral (Figure 3F) and its aggregate are commonly grey.

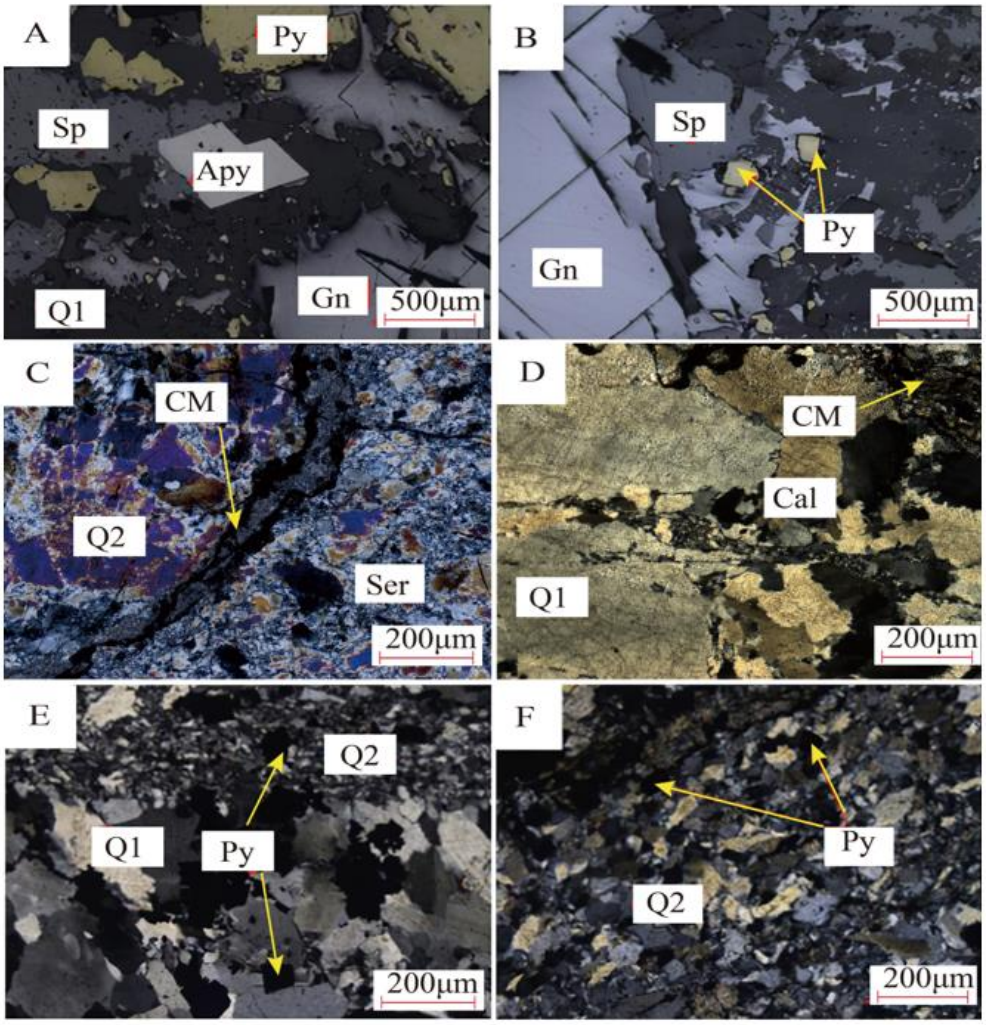

Figure 3. Photographs showing the mineral assemblages in the Bumo deposit. (A-B) Pyrite and arsenopyrite associated with galena, sphalerite and white quartz (Q1; reflected-light); (C) CM crosscut and replaced by greyish quartz (Q2) and sericite; (D) Calcite crosscut white quartz (Q1); (E) white quartz (Q1) crosscut by greyish quartz (Q2) associated with pyrite; (F) Greyish quartz (Q2) and pyrite. Apy, arsenopyrite; Py, pyrite; Sp, sphalerite; Gn, galena; Q, quartz; Ser, sericite; Cal, calcite.

Two types of CM are recognized based on field work, hand specimen and microscope observations, i.e., layered and veinlet CM. Layered CM occurred in the footwall of gold-bearing quartz veins, and the thickness can be up to one meter (Figures 4A-B). The mineral of layered CM generally shows a stringy shape (Figure 4C) and has laminate structure (Fig. 4D). More importantly, sulfides generally precipitated along the boundary between quartz veins and layered CM (Figure 4E). Veinlet CM, crosscutting the early white quartz (Q1) grains (Figures 4F-G), constitute micro veins together with Au and sulfides (Figure 4H). Under SEM, veinlet CM exhibits the shape of isometric particles (Figure 4I).

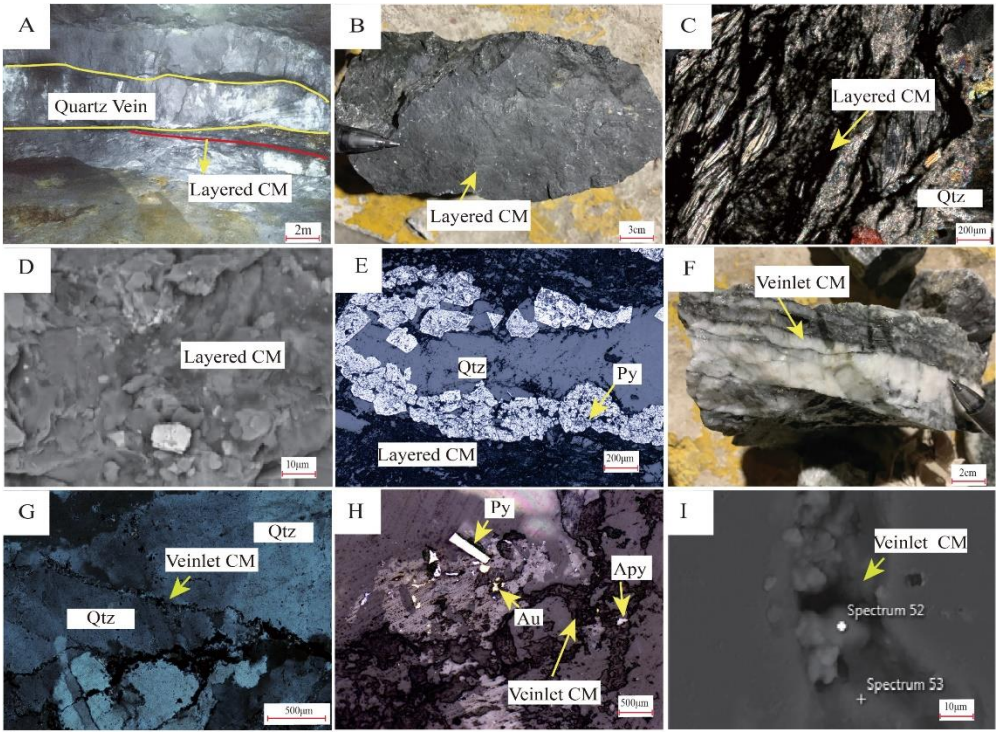

Figure 4. Photographs of the layered and veinlet CMs from the Bumo gold deposit. (A) Quartz vein and layered CM coexisting in the ore body; (B) Layered CM interlayer; (C) Filamentous particles of layered CM in quartz veins; (D) SEM image of layered CM; (E) Layered CM with sulfides(all in black seams) formed in quartz veins; (F) Detail of veinlet CM in a quartz veins; (G) Veinlet CM through the large coarse quartz particles; (H) Bright point within the veinlet CM with Au and sulfides; (I) SEM image of veinlet CM. Qtz, quartz; Au, gold; Apy, arsenopyrite; Py, pyrite.

4. Samples and analytical methods

A total twenty-four samples were collected form the No. 2 orebody in the Bumo deposit. All samples were prepared as polished thin sections and used for scanning electron microscope (SEM) and laser Raman analysis. Layered CM was extracted from CM-bearing rock samples, and they are milled to below 200 mesh powder for carbon isotope and XRD analysis. About 50g of each samples were ground under ethanol for 5 min, such that short time of pulverized would not affect the structure of layered CM. The chemical separation of layered CM samples were performed using a standard procedure using hydrochloric (HCL) and hydrofluoric(HF) acid treatment, thereafter heavy-liquid separation [31].

4.1. Petrography and scanning electron microscopy

The petrographic observation of the layered and veinlet CMs were conducted by using digital microscope and Scanning Electron microscope (SEM) on polished thin sections. Meanwhile we coated with 10-20 nm of gold in thin sections for SEM analysis. The resolution was setting 1.0 nm with a 15 kV light. The resolution is set at 1.0 nanometers and 15 kilovolts of light. The electronic photograph was taken by an electron beam exposure machine under the conditions of 15 kV acceleration voltage, 240 mA filament current and 3.5 mm beam diameter. [32].

4.2. Raman carbonaceous material geothermometer

Raman spectra were measured by Renishaw inVia Reflex Raman spectrometer (Renishaw, U.K.) at State Key Laboratory of Nuclear Resources and Environment (East China University of Technology) with a resolution of 0.5 cm^{-1}. He–Ne (λ=633 nm) laser is used as the excitation source and is focused onto a sample with the Raman spectra of cylindrical lens have been recorded at normal temperature with perpendicular and parallel polarization of incident and scattered beams. Raman spectra is a

useful non-destructive tool for calculated the maturity of organic matter [33,34]. Advances in instrument and data processing software have promote increased applications of Raman spectroscopy, and this technique was simple, fast and can be performed directly on petrographic thin sections or solid kerogen at present.

Specifically, Raman spectrum has two bands, namely G (order) and D (disorder), which are related to the maturity of the nonrandom structure of the disorder domain in the organic matter. The D and G bands can demonstrate that relevance with geological processes temperature between 200°C and 650°C [33,34]. The G band is the only Raman vibration peak in pure graphite at about 1582 cm^{-1} and it is related to the in-plane vibration of the carbon atoms in the pure graphite. The D band which located on 1350 cm^{-1} becomes active in amorphous carbon, and its frequency depends on the laser beams. The result of a double resonance Raman scattering process which was confirmed source. Beyssac et al. (2002)[33] indicates that there are additional band in the Raman spectrum of coal mine: the D2 band was observed as a small peak in the G band peak at approximately 1620 cm^{-1}. These bands are ascribed to out-of-plane defects from tetrahedral carbons, or to small crystallite size. With increase of graphitization degree, the G band becomes stronger than the D band and decided the degree of structural order increases with temperature, which is also the basis of the geothermal meter [33,34]. The degree of structural order in CM is depend on two ratios: R1 (the specific value of disordered peaks height divided by ordered peaks height) and R2 (the specific value of disordered peaks area divided by ordered peaks area).

$$R1 = \frac{D1}{G} \text{ (Height)} \quad (1)$$

$$R2 = \frac{D1}{G+D1+D2} \text{ (Area)} \quad (2)$$

Where indices Area and Height mean that the ratio on the basis of the band area and height. By using the R2 ratio, Beyssac et al., (2002) suggested R2 ratio is an important parameter in metamorphic thermometer. They proved that the crystallinity of CM is strongly correlated with the peak metamorphic temperature and not concerned with the meta-morphic pressure. Their thermometer is designed according to the linear relationship between the metamorphic temperature and parameter R2:

$$T(°C) = -445R2 + 641 \quad (3)$$

On the other hand, Rahl et al. (2005) suggested a modified thermometer based on parameters R1 and R2, which is applicable in the temperature range of 100-650°C with the fit parameter R2 more than 90%:

$$T(°C) = -737.3 + 320.9R1 - 1067R2 - 80.3638R1^2 \quad (4)$$

4.3. X-Ray diffractometry (XRD)

The XRD patterns of layered CM was conducted using Bruker D8 Advance X-ray powder diffractometer with Cu Kα radiation (λ = 0.154 nm) in State Key Laboratory of Nuclear Resources and Environment (East China University of Technology). The samples were setup on a low-background spinning specimen holder. In order to identify residual or newly formed mineral phases after hydrochloric (HCL) and hydrofluoric (HF) acid treatment, the XRD analysis in the range of 10–70°of 2θ were conducted and until were identified in all layered CM samples. The step-scanned powder diffraction data were processed by the XFIT program [35], applying the split asymmetric Pearson profile shape function to yield the peak positions and full width at half maximum (FWHM) values. It is used for fitting the broad peak profile partially integrated into the background.

4.4. Carbon stable isotopes

For measurement of layered CM samples stable carbon isotopes, we extracted ~20 g powder was put into pure orthophosphoric acid (H_3PO_4) at 75°C for 3 hours to extract CO_2 gas. The evolved CO_2 gas was injected into a Finnigan MAT-253 stable isotope mass spectrometer and carrier helium gas.

Peer-reviewed version available at Minerals 2020, 10, 708; doi:10.3390/min10080708

The China standard (GBW04405) has been calibrated using the NBS19 standard, which is used to calibrate $\delta^{13}C$ data relative to the V-PDB scale. Results are given in standard δ- notation relative to the V-PDB international standard for $\delta^{13}C$ [36]. The analysis accuracy based on standard reproducibility was better than ± 0.2% for $\delta^{13}C$ and measurements, respectively (1σ). These measurements were carried out at State Key Laboratory of Nuclear Resources and Environment (East China University of Technology).

5. Result

5.1. Raman spectra of CM

There is two notable difference between the Raman bands of the layered and veinlet CMs. Layered CM has a lower D1 band peak than G band, as well as an independent D2 band peak (Figure 5A). D1 and G bands of veinlet CM have similar peak heights and areas, and a D2 band appears only as a weak shoulder on the high wavenumber side of G band. (Figure 5B). We collected all of layered and veinlet CMs Raman spectra data, and the calculated R1 and R2 ratios for all samples are shown in Table1.

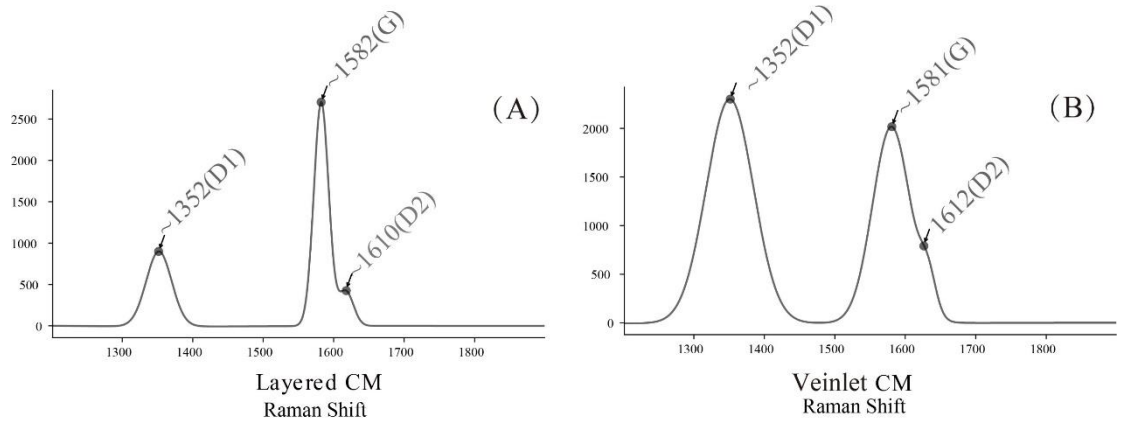

Figure 5. (A) Raman spectrum of layered CM; (B) Raman spectrum of veinlet CM (modified after Hu et al . 2015[1]).

Previous research indicates that graphitization of CM increase with temperatures, and R2 ratios decrease significantly with rising temperature [37,38]. In our study, the R2 values and temperatures are linearly correlated (Figure 6B). Meanwhile, layered CM has lower R1 and R2 ratios than veinlet CM (Table 1, Figures 6A-C). Two different calibration equations both indicate similar temperature ranges. Raman geothermometer indicate that the layered and veinlet CMs were formed at 400 – 550°C and 200 – 350°C, respectively (Figure 6D).

5.2. XRD patterns of layered CM

The X-ray diffraction analysis can be used to interpret spectrometric characteristics at different d_{002} and 2θ value, and determine the degree of graphitization [38]. Previous studies show that the d_{002} values decrease with increasing graphitization. Figure 7A shows the d_{002} decreased continuously from 3.350 Å to 3.375 Å in layered CM samples, and all of them belong to the prehnite pumpellyite facies and amphibolite-facies. The presence of high crystallinity layered CM samples are indicative of their formation under a high-temperature (400°C-higher) environment. Furthermore, XRD patterns showed that layered CM samples were accompanied together with ankerite and pyrite (Figure 7B).

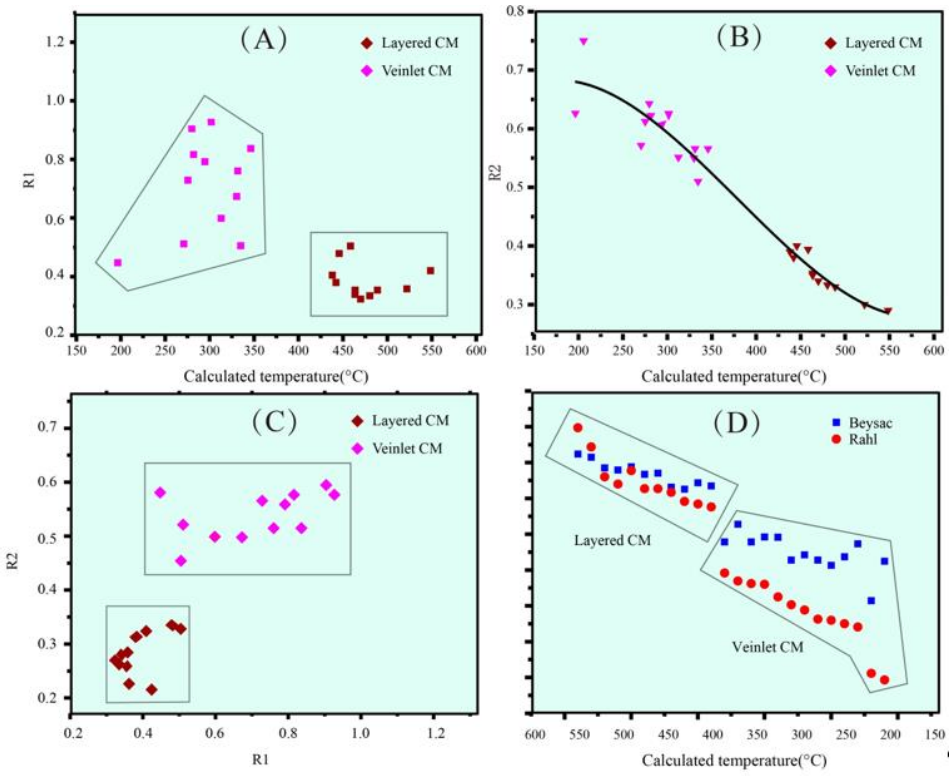

Figure 6. (A-B) R2 and R1 versus independently estimated temperature. The different colors correspond to different types of CM. We demonstrate a linear correlation in R2 over the range 150 to 600°C, but there is a little variation in R2 for temperatures over low temperatures. In contrast, R1 increases over the low-temperature range; (C) Correlation between temperature and the Raman R1, R2 ratios for layered and veinlet CM particles. The R1 and R2 ratios of CM particles from the Bumo deposit are given for comparison; (D) Metamorphic temperature calculated from the Raman R2 value after Beyssac et al. (2002)[33] compare with metamorphic temperature calculated from the Raman R1 and R2 values after Rahl et al. (2005)[34].

5.3. Stable carbon isotopic analysis of layered CM

Seventeen samples from layered CM were analyzed for stable carbon isotopic analysis, and the $\delta^{13}C$ values are -20 to -27% (VPDB). As shown in Figure 8, all these data are plotted in the region of organic carbon. Previous research demonstrates that isotopic exchange kinetics in CM is sluggish, so subsequent hydrothermal fluids are not affected the isotopic composition of CM [39].

6. Discussion

6.1. The genesis of layered and veinlet CM

Many researchers indicates that CM can be formed by metamorphism of sedimentary rocks with high organic matter contents [40]. The organic matters initially contained in the sediments can be quite different, such as lacustrine and marine algae [41]. Under the influences of metamorphism, organic matters can be decomposed into biopolymers, which can be latter polycondensation reactions into geopolymers. CM was finally generated after the metasediments rich in geopolymers (such as black shales) went through brittle-ductile deformation in shear zone [37], and produced in this way generally occurs as thick layers up to several meters thick and commonly distributed in the footwall [42], and this CM common produced by metamorphism generally present as black and grayish brown plate-like substances on hand specimens and flocculent body in microscopic images [43]. The generation commonly required the metamorphic grade with temperatures up to 400-550 °C [43].

Peer-reviewed version available at Minerals 2020, 10, 708; doi:10.3390/min10080708

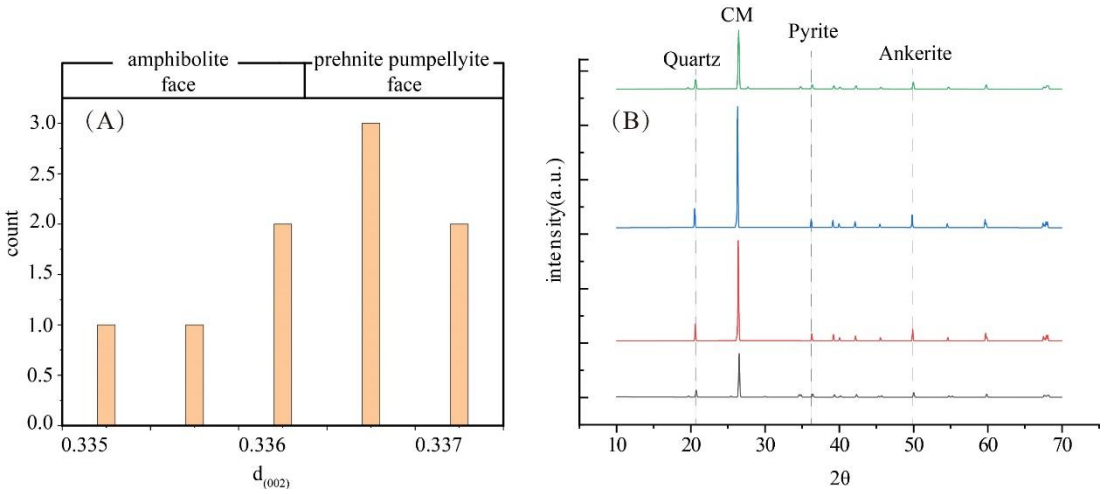

Figure 7. (A) XRD parameters of $d_{(002)}$ graphitic peak of layered CM from the Bumo deposit; (B) XRD patterns of the layered CM, accompanied by a high graphitic peak intensity at 25.6° and other mineral peak intensity characteristic.

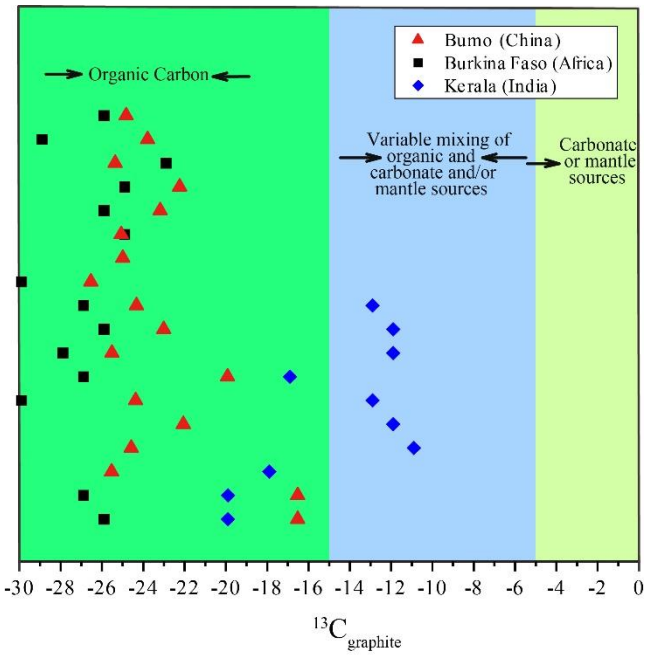

Figure 8. Frequency distribution of $\delta^{13}C$ values of layered CM from the Bumo deposit and compared with different gold deposit.

The alternative genesis for CM is via redox reaction between CO_2- and CH_4-bearing hydrothermal fluids in ore deposits. In the process of fluid infiltration, the geological process will drop the amount of CO_2 and CH_4 in fluids [44]. This CM generated by hydrothermal fluids is composed of tiny isometric particles with sizes lower than 5 mm, and have highly disorder in SEM image. However, they also form veinlets locally along with quartz, carbonate and ore-bearing sulfides. Besides, this CM associated with hydrothermalism is commonly formed instantly under low temperatures, so there is far less time for CM to accumulate impurities, different from CM which produced by metamorphism, which develops over millions of years [7].

Layered CM commonly occurred in the footwall of fault in the Bumo deposit (Figure 4A), and present as flocculent textures under microscope. Raman carbonaceous material geothermometer indicates that layered CM is formed at 450 – 550°C (Figure 6D), consistent with the d_{002} values of 3.35

– 3.375 obtained by XRD analysis (Figure 7). Previous fluid inclusion research suggests that the Bumo deposit is form at 180-350 °C [45], significantly lower temperature of layered CM. Meanwhile, the Baoban group went through greenschist- to amphibolite-grade metamorphism during Caledonian [28] which reach up to 500 °C [12,16], similar to that of layered CM. In addition, $\delta^{13}C$ values of layered CM, ranging from -20 to -27%, demonstrate the origin of organic carbon [46]. Consequently, layered CM was interpreted to be generated by metamorphism of the Baoban group during Caledonian, transferring the organic matter dispersed into graphite [20].

Different from layered CM, veinlet CM generally occurs in ore-bearing quartz veins [47]. Veinlet CM grains with complete spherical structures in SEM image form micro-veins with Au, arsenopyrite and pyrite, crosscutting early large quartz grains. Raman carbonaceous material geothermometer demonstrates that veinlet CM was formed at 200–300 °C, consistent with the gold mineralization and significantly lower than layered CM. Consequently, veinlet CM is likely to be hydrothermal origin. Previous research indicates that the ore fluids of the gold deposits in the Gezhen shear zone are rich in CO_2 [28], and altered host rocks have high contents of hydrocarbon gas (such as CH_4, H_2 and C_2H_4). Veinlet CM was interpreted to be formed by following two redox reactions [48] :

$$CH_{4(g)} + CO_{2(g)} = 2C + 2H_2O_{(l)} \quad (5)$$

$$6H_{2(g)} + 2CO_{2(g)} = C + CH_{4(g)} + 4H_2O_{(l)} \quad (6)$$

6.2. Implication for gold mineralization

Two types of CM with multiple genesis are commonly discovered in many hydrothermal gold deposits [49]. CM with metamorphic origin is ideal reducing agent for Au and sulfide precipitation. In addition, some scholars proposed that Au particles were initially absorbed by CM grains in Precambrian metasediments, and was later leached by ore fluids. These pre-ore CM is also physically weak, and is prone to faulting and provide space for ore fluid precipitation [7]. As for CM with hydrothermal origin, its co-precipitation with sulfides altered the pH of ore fluids, led to the destabilization of Au complexes [50].

In the Bumo deposit, as a criterion for ore prospecting, layered CM is generally accompanied by gold-bearing ore veins. More importantly, gold-bearing sulfides are concentrated along the boundaries between the quartz veins and layered CM. Consequently, the spatial association between layered CM and gold in quartz veins does indicates gold deposition affected by a redox reaction with layered CM through the chemical reaction 7 [5]. Veinlet CM occurs as micro-veins together with sulfides and gold, and they are produced by reaction 8 [7,51,52].

$$4Au(HS)^-_{2(aq)} + C_{(s)} + 4H^+_{(aq)} + 2H_2O_{(l)} = 4Au_{(s)} + CO_{2(aq)} + 8H_2S_{(aq)} \quad (7)$$

$$2FeO_{(s)} + 4H_2S_{(aq)} + CO_{2(aq)} = 2FeS_2 + C_{(s)} + 4H_2O_{(l)} \quad (8)$$

Based on the above description, the mineralization model for the Bumo gold deposit is outlined as: 1) Layered CM was formed by the pre-ore Caledonian metamorphism at the temperatures of 450 – 550°C, and this CM is physically weak, leading stress concentration and shear deformation; 2) The reducing environment and space provided by layered CM promoted the ore mineral precipitation (Figure 9A); 3) Veinlet CM is also produced by the water-rock interaction at 200 – 350°C, coeval with sulfides and gold (Figure 9B).

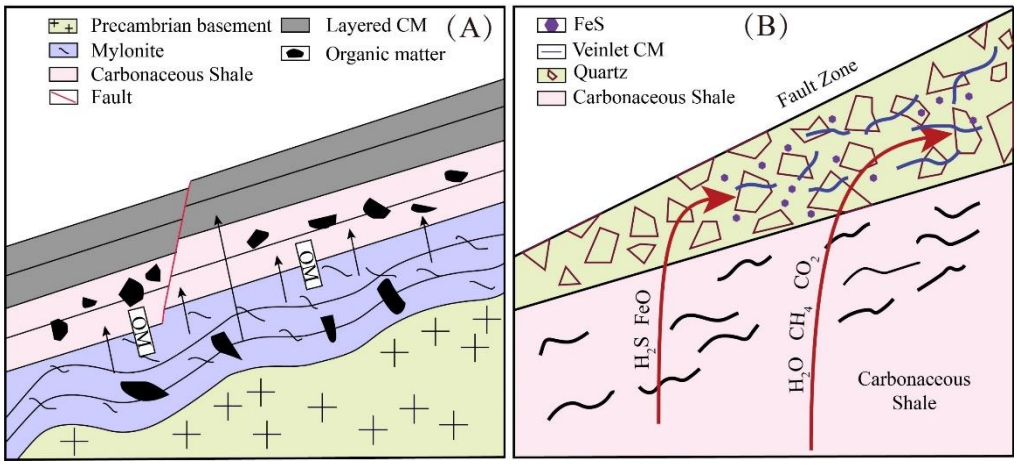

Figure 9. Schematic diagram showing the evolution of two types of CM in the Bumo deposit. The diagram was created for the current study (modified after KIRILOVA et al. 2018 and Wu et al. 2020[48,52]).

7. Conclusions

(1) Two types of CM occur in the Bumo gold deposit, i.e., layered and veinlet CMs. Layered CM has laminate structure, was formed at 450 – 550°C and sourced from organic matter, and through pre-ore Caledonian metamorphism. In contrast, veinlet CM has isometric shape and was formed at 200 – 350°C, and through syn-ore hydrothermalism.

(2) Layered CM promoted the shear deformation of host rocks and provided a reducing environment, favorable for gold mineralization. Veinlet CM coprecipitated with sulfides and gold.

Supplementary Materials: The following are available online at https://zenodo.org/record/3911133. Table 1: Raman spectroscopy data of layered and veinlet CM samples from the Bumo deposit. Table 2. Stable isotopic composition of layered CM samples from the Bumo deposit.

Author Contributions: Z.D. designed the project; T.D., D.X., Z.L., and S.Z. collected the samples; Y.H., L.L., and K.X. performed the Raman analyses and reduced the data; Z.D. and T.D. wrote and organized the paper, with a careful discussion and revision by D.X. All authors discussed the results and evaluated the data. All authors have read and agreed to the published version of the manuscript.

Funding: The paper was financially co-supported the National Natural Science Foundation of China (Nos. 41930428, 41472171, 41672077, 41302049), the DREAM project of MOST China (No. 2016YFC0600401), the Chinese Ministry of Land and Resources (No. 200646092), the Open Research Fund Program of Key Laboratory of Metallogenic Prediction of Nonferrous Metals and Geological Environment Monitoring (Central South University), Ministry of Education (Nos. 2019YSJS02, 2019YSJS12), Open Research Fund Program of State Key Laboratory of Nuclear Resources and Environment, East China University of Technology (No. NRE1915) and Jiangxi province graduate student innovation special fund project (YC2019-S271). We are thankful for the assistance from reviewers.

Acknowledgments: We are thankful for the assistance from reviewers. A particular thank is given to Hainan Geological Survey Institute and Zhaojin mining company for their help in the field investigation.

Conflicts of Interest: The authors declare no conflict of interest.

References:

1. Hu, S.; Evans, K.; Craw, D.; Rempel, K.; Bourdet, J.; Dick, J.; Grice, K. Raman characterization of carbonaceous material in the Macraes orogenic gold deposit and metasedimentary host rocks, New Zealand. *Ore Geol Rev* **2015**, 70, 80-95
2. Mirasol-Robert, A.; Grotheer, H.; Bourdet, J.; Suvorova, A.; Grice, K.; McCuaig, T.C.; Greenwood, P.F. Evidence and origin of different types of sedimentary organic matter from a Paleoproterozoic orogenic Au deposit. *Precambrian Res* **2017**, 299, 319-338

3. Kříbek, B.; Sýkorová, I.; Machovič, V.; Knésl, I.; Laufek, F.; Zachariáš, J. The origin and hydrothermal mobilization of carbonaceous matter associated with Paleoproterozoic orogenic-type gold deposits of West Africa. *Precambrian Res* **2015**, 270, 300-317
4. Berge, J. Paleoproterozoic, turbidite-hosted, gold deposits of the Ashanti gold belt (Ghana, West Africa): Comparative analysis of turbidite-hosted gold deposits and an updated genetic model. *Ore Geol Rev* **2011**, 39, 91-100
5. Cox, S.F.; Sun, S.S.; Etheridge, M.A.; Wall, V.J.; Potter, T.F. Structural and geochemical controls on the development of turbidite-hosted gold quartz vein deposits, Wattle Gully mine, central Victoria, Australia. *Econ Geol* **1995**, 90, 1722-1746
6. Craw, D.; Windle, S.J.; Angus, P.V. Gold mineralization without quartz veins in a ductile-brittle shear zone, Macraes Mine, Otago Schist, New Zealand. *Miner Deposita* **1999**, 34, 382-394
7. Craw, D.; MacKenzie, D.; Grieve, P. Supergene gold mobility in orogenic gold deposits, Otago Schist, New Zealand. *New Zeal J Geol Geop* **2015**, 58, 123-136
8. Upton, P.; Craw, D. Modelling the role of graphite in development of a mineralised mid-crustal shear zone, Macraes mine, New Zealand. *Earth Planet Sc Lett* **2008**, 266, 245-255
9. Liang. The origin and geology of the tuwaishan gold deposit in hainan province. *Geological Bulletin of China* **1992**, 11
10. Xia, Y.; Wu, X.; Yang, Y. Fluid inclusion studies of gold deposits in the Gezhen shear zone, Hainan Province, China. *Chinese Journal of Geochemistry* **1995**, 14, 371-380
11. Ding. The tectonic evolution of the gezhen fault zone and its gold meneralization series [j]. *Contributions to geology and mineral resouces research* **1994**, 3 (In Chinese with English Abstract)
12. Xu, D.; Wang, Z.; Wu, C.; Zhou, Y.; Shan, Q.; Hou, M.; Fu, Y.; Zhang, X. Mesozoic gold mineralization in Hainan Province of South China: Genetic types, geological characteristics and geodynamic settings. *J Asian Earth Sci* **2017**, 137, 80-108
13. Ding, S.J. Fractal analysis on fault system in central and western HaiNan gold metallogenic province. *Earth Science Frontiers* **2004**, 11, 189-194 (In Chinese with English Abstract)
14. Wang, Z.; Xu, D.; Hu, G.; Yu, L.; Wu, C.; Zhang, Z.; Cai, J.; Shan, Q.; Hou, M.; Chen, H. Detrital zircon U–Pb ages of the Proterozoic metaclastic-sedimentary rocks in Hainan Province of South China: New constraints on the depositional time, source area, and tectonic setting of the Shilu Fe–Co–Cu ore district. *J Asian Earth Sci* **2015**, 113, 1143-1161
15. Chen, B.L. Geochemical tracer studies on the isotopes from the gold deposits, Hainan. *journal of earth* **1996**, 3 (In Chinese with English Abstract)
16. Xu, D.R.; Xia, B.; Li, P.C.; Chen, G.H.; Ma, C.; Zhang, Y.Q. Protolith natures and U‐Pb sensitive high mass‐resolution ion microprobe (SHRIMP) zircon ages of the metabasites in Hainan Island, South China: Implications for geodynamic evolution since the late Precambrian. *Isl Arc* **2007**, 16, 575-597 (In Chinese with English Abstract)
17. Xu, D.; Wang, Z.; Cai, J.; Wu, C.; Bakun-Czubarow, N.; Wang, L.; Chen, H.; Baker, M.J.; Kusiak, M.A. Geological characteristics and metallogenesis of the Shilu Fe-ore deposit in Hainan Province, South China. *Ore Geol Rev* **2013**, 53, 318-342
18. Zou, S.; Yu, L.; Yu, D.; Xu, D.; Ye, T.; Wang, Z.; Cai, J.; Liu, M. Precambrian continental crust evolution of Hainan Island in South China: constraints from detrital zircon Hf isotopes of metaclastic-sedimentary rocks in the Shilu Fe-Co-Cu ore district. *Precambrian Res* **2017**, 296, 195-207
19. Li, X.; Hanguang, L.; Yijun, Z.; Huiyu, Z.; Aijun, P. Diagenesis and Mineralization of Gold Deposits in Gezhen Gold Ore Belt, Hainan. *Mineral Deposits* **2002**, 21, 719-722 (In Chinese with English Abstract)
20. Zhan; Shuhai, Z.; Guoqing, L. The Gezhen auriferous shear zone and related metallogenic series in western Hainan Island. *Mineral Deposits* **1996**, 4 (In Chinese with English Abstract)
21. Xu, D.R.; Liang, X.Q.; Cheng, G.H.; HUANG, Z.; HU, H. Research on the geochemistry and genesis of mesoproterozoic granites on hainan island. *Geotectonica et Metallogenia* **2001**, 25, 420-433
22. Chen, Y. Hercynian and Indosinian structureal overprinting and 40Ar-39Ar geochronology of Hainan Island-South China. Doctor Type, The Chinese Academy of Sciences, 2006. (In Chinese with English Abstract)
23. Wang, P.; Kaneda, H.; Ding, S.; Zhang, X.; Liao, X.; Dong, F.; Li, Z.; Liu, X.; Lai, Y. Geology and mineralogy of the Baolun hydrothermal gold deposit in the Hainan Island, South China. *Resour Geol* **2006**, 56, 157-166 (In Chinese with English Abstract)

24. Liang. Sm-Nd Ages of the Precambrian Granitic-Greenstone Series in Hainan Island and their Geological Significance [J]. *Acta Petrol Sin* **1995**, 1 (In Chinese with English Abstract)
25. Rao, D.; Xiang-ding, H.; Shao-xiong, T.U. Metallogenetic evolution of the Gezhen gold deposit belt in western Hainan Island, China: With the main deposits in Erjia-Bumo area as examples. *Geology and Mineral Resources of South China* **1996**, 3, 12-22 (In Chinese with English Abstract)
26. Li, X.; Li, Z.; Li, W.; Wang, Y. Initiation of the Indosinian Orogeny in South China: evidence for a Permian magmatic arc on Hainan Island. *The Journal of geology* **2006**, 114, 341-353 (In Chinese with English Abstract)
27. Yu, L.; Zou, S.; Cai, J.; Xu, D.; Zou, F.; Wang, Z.; Wu, C.; Liu, M. Geochemical and Nd isotopic constraints on provenance and depositional setting of the Shihuiding Formation in the Shilu Fe–Co–Cu ore district, Hainan Province, South China. *J Asian Earth Sci* **2016**, 119, 100-117
28. Ding. Gezhen detachment fault zone and its mineralization, the west hainan province [j]. *Contributions to Geology and Mineral Resources Research* **1991**, 1
29. Yu. Geological characteristics and genesis of the Baoban gold deposit, in ductile shear zone-type gold deposits in the Cathysian block. In Beijing, Science Press: 1992.
30. Zhou, Y.; Hou, M. Gold Ore Deposits in the Gezhen Metallogenic Belt, Hainan Province of South China: An Example of Orogenic-Type Deposit? *Acta Geologica Sinica - English Edition* **2014**, 88, 338-339 (In Chinese with English Abstract)
31. Lewan, M.D.; Bjorøy, M.; Dolcater, D.L. Effects of thermal maturation on steroid hydrocarbons as determined by hydrous pyrolysis of Phosphoria Retort Shale. *Geochim Cosmochim Ac* **1986**, 50, 1977-1987
32. Pye, K.; Krinsley, D.H. Petrographic examination of sedimentary rocks in the SEM using backscattered electron detectors. *J Sediment Res* **1984**, 54, 877-888
33. Beyssac, O.; Goffé, B.; Chopin, C.; Rouzaud, J.N. Raman spectra of carbonaceous material in metasediments: a new geothermometer. *J Metamorph Geol* **2002**, 20, 859-871
34. Rahl, J.M.; Anderson, K.M.; Brandon, M.T.; Fassoulas, C. Raman spectroscopic carbonaceous material thermometry of low-grade metamorphic rocks: Calibration and application to tectonic exhumation in Crete, Greece. *Earth Planet Sc Lett* **2005**, 240, 339-354
35. Coelho, A.A.; Cheary, R.W.; Smith, K.L. Analysis and structural determination of Nd-substituted zirconolite-4M. *J Solid State Chem* **1997**, 129, 346-359
36. Parker, P.L. The biogeochemistry of the stable isotopes of carbon in a marine bay. *Geochim Cosmochim Ac* **1964**, 28, 1155-1164
37. Orberger, B.; Vymazalova, A.; Wagner, C.; Fialin, M.; Gallien, J.P.; Wirth, R.; Pasava, J.; Montagnac, G. Biogenic origin of intergrown Mo-sulphide-and carbonaceous matter in Lower Cambrian black shales (Zunyi Formation, southern China). *Chem Geol* **2007**, 238, 213-231
38. Nakamura, Y.; Akai, J. Microstructural evolution of carbonaceous material during graphitization in the Gyoja-yama contact aureole: HRTEM, XRD and Raman spectroscopic study. *J Miner Petrol Sci* **2013**, 108, 131-143
39. Binu-Lal, S.S.; Kehelpannala, K.V.W.; Satish-Kumar, M.; Wada, H. Multistage graphite precipitation through protracted fluid flow in sheared metagranitoid, Digana, Sri Lanka: evidence from stable isotopes. *Chem Geol* **2003**, 197, 253-270
40. Leventhal, J.S.; Grauch, R.I.; Threlkeld, C.N.; Lichte, F.E.; Harper, C.T. Unusual organic matter associated with uranium from the Claude deposit, Cluff Lake, Canada. *Econ Geol* **1987**, 82, 1169-1176
41. Burhan, R.; Trendel, J.M.; Adam, P.; Wehrung, P.; Albrecht, P.; Nissenbaum, A. Fossil bacterial ecosystem at methane seeps: origin of organic matter from Be'eri sulfur deposit, Israel. *Geochim Cosmochim Ac* **2002**, 66, 4085-4101
42. Oohashi, K.; Hirose, T.; Shimamoto, T. Shear-induced graphitization of carbonaceous materials during seismic fault motion: Experiments and possible implications for fault mechanics. *J Struct Geol* **2011**, 33, 1122-1134
43. Jehlička, J.; Urban, O.; Pokorný, J. Raman spectroscopy of carbon and solid bitumens in sedimentary and metamorphic rocks. *Spectrochimica Acta Part A: Molecular and Biomolecular Spectroscopy* **2003**, 59, 2341-2352

44. Wu, Y.; Evans, K.; Fisher, L.A.; Zhou, M.; Hu, S.; Fougerouse, D.; Large, R.R.; Li, J. Distribution of trace elements between carbonaceous matter and sulfides in a sediment-hosted orogenic gold system. *Geochim Cosmochim Ac* **2020**, 276, 345-362
45. Tu; Gao. Ore-forming fluids and stable isotope geochemistry of several gold deposits in southwestern hainan island [j]. *Mineral Deposits* **1993**, 4
46. Dissanayake, C.B.; Chandrajith, R. Sri Lanka–Madagascar Gondwana linkage: evidence for a Pan-African mineral belt. *The Journal of Geology* **1999**, 107, 223-235
47. Kresse, C.; Lobato, L.M.; Hagemann, S.G.; Figueiredo E Silva, R.C. Sulfur isotope and metal variations in sulfides in the BIF-hosted orogenic Cuiabá gold deposit, Brazil: Implications for the hydrothermal fluid evolution. *Ore Geol Rev* **2018**, 98, 1-27
48. Manning, C.E.; Shock, E.L.; Sverjensky, D.A. The chemistry of carbon in aqueous fluids at crustal and upper-mantle conditions: experimental and theoretical constraints. *Reviews in Mineralogy and Geochemistry* **2013**, 75, 109-148
49. Goldfarb, R.; Baker, T.; Dube, B.; Groves, D.I.; Hart, C.J.; Gosselin, P. Distribution, character and genesis of gold deposits in metamorphic terranes. In Society of Economic Geologists: 2005.
50. Almodóvar, G.R.; Sáez, R.; Pons, J.M.; Maestre, A.; Toscano, M.; Pascual, E. Geology and genesis of the Aznalcóllar massive sulphide deposits, Iberian Pyrite Belt, Spain. *Miner Deposita* **1997**, 33, 111-136
51. Hu, S.; Evans, K.; Craw, D.; Rempel, K.; Grice, K. Resolving the role of carbonaceous material in gold precipitation in metasediment-hosted orogenic gold deposits. *Geology* **2017**, 45, 167-170
52. Kirilova, M.; Toy, V.G.; Timms, N.; Halfpenny, A.; Menzies, C.; Craw, D.; Beyssac, O.; Sutherland, R.; Townend, J.; Boulton, C. Textural changes of graphitic carbon by tectonic and hydrothermal processes in an active plate boundary fault zone, Alpine Fault, New Zealand. *Geological Society, London, Special Publications* **2018**, 453, 205-223